Paleoceanography and Paleoclimatology

RESEARCH ARTICLE
10.1029/2024PA004935

Upper Ocean Instability in the Subpolar North Atlantic and Its Implications for Deep Water Formation During Interglacials

Benoit Thibodeau[1,2], John M. Doherty[2,3], Montserrat Alonso-García[4,5], Shraddha Band[6], Alba González-Lanchas[7], Christelle Not[8], and Haojia Ren[6]

[1]Department of Earth and Environmental, The Chinese University of Hong Kong, Sha Tin, Hong Kong, [2]School of Life Sciences, The Chinese University of Hong Kong, Sha Tin, Hong Kong, [3]Now at Environmental Law Institute and The Earth Commons, Georgetown University, Washington, DC, USA, [4]Department of Geology- Paleontology, University of Salamanca, Salamanca, Spain, [5]CCMAR, Centro de Ciências do Mar, Universidade do Algarve, Faro, Portugal, [6]Department of Geosciences, National Taiwan University, Taipei, Taiwan, [7]Department of Earth Sciences, Oxford University, Oxford, UK, [8]Department of Earth Sciences and Swire Institute of Marine Sciences, The University of Hong Kong, Pokfulam, Hong Kong

Key Points:

- Surface conditions became unstable post-climate optimum during MIS 11
- Cold conditions peak around 390 ka and are associated with a deep mixed layer, presence of IRD and strong seasonality
- Surface instability and cold event are associated with a decrease in deep water ventilation in the North Atlantic

Correspondence to:
B. Thibodeau,
benoit.thibodeau@cuhk.edu.hk

Citation:
Thibodeau, B., Doherty, J. M., Alonso-García, M., Band, S., González-Lanchas, A., Not, C., & Ren, H. (2025). Upper ocean instability in the subpolar North Atlantic and its implications for deep water formation during interglacials. *Paleoceanography and Paleoclimatology*, *40*, e2024PA004935. https://doi.org/10.1029/2024PA004935

Received 5 JUN 2024
Accepted 26 JAN 2025

Abstract In this multiproxy study, we used new isotopic data on planktonic foraminifera to highlight the strong instability that characterized surface conditions in the Iceland Basin during Marine Isotope Stage 11 (MIS 11). We produced new oxygen isotope data on the planktonic species *Neogloboquadrina incompta* and *Turborotalita quinqueloba*, foraminifera-bound nitrogen isotope data on *N. incompta*, and calcareous nannofossil data at coring site IODP Site U1314. The multiproxy record displays two distinct upper ocean regimes: a relatively stable pre-climate optimum and an unstable post-climate optimum with high amplitude variations in nutrient utilization and seasonality proxies, and strong enrichment in oxygen isotopes suggesting colder and/or saltier upper waters. The latter regime was concomitant with a resurgence in ice-rafted debris. Interestingly, this surface instability is not observed in cores from sites affected by the North Atlantic Current. Moreover, deep water ventilation is reconstructed to decrease throughout the eastern North Atlantic, while remaining rather constant in the Labrador Sea. The evidence presented here indicates that deep-water formation was unstable throughout MIS 11, and that peak periods of deep-water formation varied across high latitude North Atlantic basins, depending on the prevailing surface conditions in each region. These findings suggest that reconstructing deep-water formation and ventilation require a comprehensive approach that accounts for the interconnectivity between different components of the overturning circulation system.

Plain Language Summary Deep-water formation is a key component of our climate system as it contributes to long-term carbon dioxide storage in the ocean. Its strong feedback effect helps modulate Earth's climate over time; warm climates are often characterized by vigorous deep-water formation, leading to efficient carbon storage, which in turn tends to cool the climate. Understanding the drivers of deep-water formation strength is crucial for forecasting the potential impact of global warming on ocean carbon storage and future climate. In this study, we use a past climate analog—a period in the past with climate characteristics similar to today—to investigate how deep-water formation responds to slightly warmer (2–4°C) global air temperatures. We found that deep-water formation varied with changes in the upper-ocean structure and shifted locations throughout the warm period studied, without collapsing. These findings will help us better understand and forecast potential changes in deepwater formation under modern global warming.

1. Introduction

The periodic variation of ice-sheet growth and decay (i.e., glacial-interglacial cycles) is one of the most prominent features of Pleistocene climate. According to the classical theory of orbital climate forcing, glacial terminations are said to arise during times of high northern-hemisphere insolation, coincident with a sufficiently large volume of northern-hemisphere ice (Imbrie et al., 1992, 1993; Peacock et al., 2006; Raymo, 1997). During such transitions, orbital-driven summertime warming triggers the melting of northern-hemisphere ice, which elevates freshwater content in the North Atlantic and weakens Atlantic circulation, specifically the Atlantic Meridional Overturning Circulation (AMOC). As a result, meridional heat transport is also altered, increasing the intensity of northern-hemisphere winters, enhancing warming in the southern hemisphere and shifting atmospheric

circulation patterns (reviewed by Denton et al., 2010). The combination of enhanced southern-hemisphere warming and a southward migration of westerlies in the southern hemisphere increases carbon-dioxide outgassing, eventually resulting in the emergence of warmer interglacial climate states (Denton et al., 2010). While this orbital-driven climate theory appears to hold for many glacial-interglacial transitions, the interglacial marine isotope stage (MIS) 11, ~424–374 ka, is a notable exception. During MIS 11, anomalously warm and long interglacial conditions arose and persisted during relatively subdued orbital forcing—a phenomenon known as the "MIS 11 paradox" (Candy et al., 2014; Droxler et al., 2003; Imbrie et al., 1993; Vázquez Riveiros et al., 2013). The apparent MIS 11 paradox has been previously explained by an "overshoot" of the AMOC, which was hypothesized to have occurred after a particularly prolonged AMOC reduction driven by extended meltwater input during the termination of the previous intense glacial interval, MIS 12 (Dickson et al., 2009). This AMOC overshoot was further hypothesized to supply additional heat to the northern hemisphere, resulting in enhanced warming despite the relatively weak regional insolation (Dickson et al., 2009; Oliveira et al., 2016; Tzedakis et al., 2022; Vázquez Riveiros et al., 2013). As such, the particularly strong AMOC during MIS 11 is considered to be a key climatic driver during this anomalous interval in Earth history (Vázquez Riveiros et al., 2013).

In addition to the initial AMOC intensification during the MIS 12 deglaciation, a secondary strengthening of the AMOC was previously identified in benthic $\delta^{13}C$ records prior to the onset of the climatic optimum, ~410–400 ka (Dickson et al., 2009). This secondary AMOC intensification was hypothesized to result from the gradual reduction of northern-hemisphere sea ice, allowing for a northward extension of surface-ocean currents (Dickson et al., 2009). Indeed, an anomalously deep summer mixed layer was maintained in the polar Nordic Seas throughout MIS 11 compared to the Holocene, which may indicate the presence of favorable hydrographic conditions for polar convection to occur (Thibodeau et al., 2017). Later reconstructions further revealed that the Nordic Seas' summer mixed layer was at its deepest position during the onset of the climatic optimum (Doherty et al., 2021). Together with data-constrained modeling, these results imply that this region likely became an important locus for driving deep-water formation and, thus, also influencing the AMOC intensification. As such, deep-water formation in the Nordic Seas likely also contributed to extending the enhanced warming of the northern hemisphere and delayed the next glacial interval, giving rise to the prolonged duration of interglacial conditions characteristic of MIS 11 (Doherty et al., 2021). While such oceanographic changes may be relevant for the increasingly warmer and ice-free North Atlantic region during MIS 11, the relative importance of deep-water formation in the Nordic Seas is not well understood due to a lack of hydrographic reconstructions from other potential convective regions.

In the contemporary ocean, a major branch of Atlantic deep-water formation occurs in the eastern subpolar North Atlantic, whereas only a minor contribution is derived from the polar Nordic Seas (Petit et al., 2020). However, modeling experiments suggest that the relative importance of deep-water formation in polar regions may increase under extreme scenarios of anthropogenic warming (Lique et al., 2018; Lique & Thomas, 2018). MIS 11 is considered to be a potential analog for Earth's contemporary climate system, due to its similarities in orbital geometry (Berger & Loutre, 2002; Loutre & Berger, 2003), preindustrial atmospheric greenhouse gas chemistry (Raynaud et al., 2005; Siegenthaler et al., 2005) and substantial reduction in Greenland Ice Sheet volume (e.g., de Vernal & Hillaire-Marcel, 2008; Reyes et al., 2014). For this reason, understanding the evolution of the different overturning branches during MIS 11 could offer a unique insight into the long-term fate of the contemporary AMOC and its implications for global climate.

Deep-water formation occurs during winter in the subpolar and polar North Atlantic due to upper-ocean buoyancy loss (Buckley & Marshall, 2016; Petit et al., 2020). This process requires an initial "preconditioning" phase, during which upper-ocean mixing is intensified (Killworth, 1983). When convection occurs, the mixed-layer depth (MLD) deepens to greater than 100 m below the sea surface. Because of this preconditioning phase, convection may reasonably be more favorable in regions with pre-existing deep summer mixed layers (i.e., relatively weak stratification). The potential link between the summer MLD and deep-water formation has inspired numerous paleo-reconstructions of upper-ocean hydrographic variability in the polar and subpolar North Atlantic regions (Bauch et al., 2011; Kandiano et al., 2017; Simstich et al., 2003, 2012; Thibodeau et al., 2017; Zhuravleva et al., 2017). Despite the ambiguous relationship between summer MLD and winter convection, paleoceanographers have relied on summer MLD reconstructions due to the absence of reliable proxies for winter MLD.

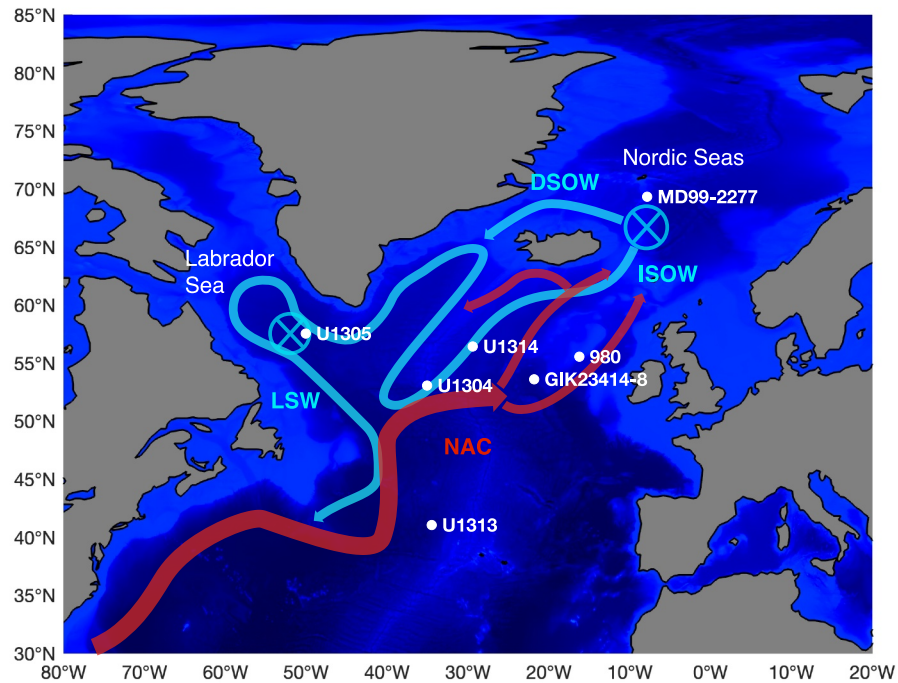

Figure 1. Simplified circulation and coring sites in the North Atlantic. This figure illustrates the location of the primary coring site for the present study (IODP site U1314), alongside the positions of additional cores used for comparison in subsequent figures. The map also depicts major ocean currents in the region, with deep water currents represented in blue and surface water currents shown in red. Acronyms are: NAC—North Atlantic Current; ISOW—Iceland-Scotland Overflow Water; DSOW—Denmark Strait Overflow Water; LSW—Labrador Sea Water.

In sum, without a complete understanding of the convective behavior of the subpolar Atlantic, our understanding of the relative importance of the Nordic Seas in driving the AMOC during the MIS 11 climatic optimum is limited. To this aim, here we present multiple new geochemical reconstructions of upper-ocean structure of the Iceland Basin (IODP site U1314; Figure 1) during MIS 11. These records include nitrogen isotopic ratios of organic matter bound within planktic foraminifera (*Neogloboquadrina incompta*), as well as carbon and oxygen isotopic ratios of two species of planktic foraminifera constrained to different upper-ocean depth habitats (*N. incompta* and *Turborotalita quinqueloba*). We supplement our interpretation of these data with additional measurements of carbon isotopic ratios in benthic foraminifera (*Cibicidoides wuellerstorfi*) to investigate changes in ventilation of the Iceland Basin during MIS 11, and a coccolithophore-derived surface primary productivity record. Because this study represents the first analysis of the younger half of MIS 11 in core U1314, we also present a new age model based on the oxygen isotopic composition of *C. wuellerstorfi* specimens correlated to the "LR04" global stack (Lisiecki & Raymo, 2005).

2. Methods

2.1. Oceanographic Setting and Foraminifera Picking

Sediment core U1314, located at 56°21.8′N, 27°53.3′W (Figure 1), was drilled during the International Ocean Discovery Program's (IODP) Expedition 306 at a depth of 2,820 m (Proceedings of the IODP, 303/306, 2006). The site is within the Gardar Drift of the Iceland Basin, a region of primary importance in the contemporary Atlantic convection (Petit et al., 2020). At the surface, this area is oceanographically affected by the North Atlantic Current (NAC) and the subpolar gyre. As the site is within the boundary of the Ruddiman ice-rafting belt (Ruddiman, 1977), one original motivation of drilling this site was to reconstruct the impact of local meltwater input on NADW formation (Proceedings of the IODP, 303/306, 2006). Further, as the benthic region here is

influenced by upstream Iceland-Scotland Overflow Water (ISOW), paleoceanographic data extracted from this core may also record variations in deep-water masses exported from the Nordic Seas in addition to the deep-water masses formed in situ (Bianchi & McCave, 2000; Van Aken & De Boer, 1995).

A total of 42 sediment core samples (WDGE), each about 20 cm^3, were supplied from the IODP Bremen Core Repository at a resolution of typically 15–25 cm. The studied MIS 11 sediment section is constrained by the ages presented in Alonso-Garcia, Sierro, and Flores (2011) and Alonso-Garcia, Sierro, Kucera, et al. (2011) and by additional reflectance and magnetic susceptibility data (Proceedings of the IODP, 303/306, 2006). Each of the core segments was freeze-dried and weighed. Then, wet sieving with Milli-Q water was conducted to remove the mud (<63 μm) fraction of the sample. The >63 μm sample was oven-dried at a temperature of 55°C and then further sieved to separate sediment fractions at the following catch sizes: >500 μm, 300–500 μm, 150–300 μm and 63–150 μm. Tests of the planktic foraminifera species, *N. incompta* and *T. quniqueloba*, and the benthic foraminifera species, *C. wuellerstorfi*, were handpicked from the 150–300 μm fraction.

2.2. $\delta^{18}O$ and $\delta^{13}C$ Analysis of Foraminifera

Approximately 50–150 μg of *N. incompta* and *T. quinqueloba* tests (typically 10 to 30 individual specimens) were handpicked under a light microscope for carbon and oxygen isotopic analysis. Approximately 10–50 μg of *C. wuellerstorfi* tests (typically 5–15 individual specimens) were also handpicked under a binocular light microscope for carbon and oxygen isotopic analysis. Stable carbon and oxygen isotopic ratios were measured on a MAT 253 isotope ratio mass spectrometer (IRMS) coupled to a Kiel IV carbonate preparation system in the Stable Isotope Lab located in the College of Earth, Ocean, and Atmospheric Sciences at Oregon State University. NBS 19 and Wiley (in-house) standards were also analyzed to normalize the data to the international Vienna Pee Dee Belemnite (VPDB; Coplen, 1995). Scale, which are presented in the conventional delta (δ) notation. Standard deviations (1σ) of replicate measurements for $\delta^{13}C$ on *N. incompta* ($n = 5$) and *T. quinqueloba* ($n = 4$) specimens averaged 0.09 and 0.15‰ respectively. For $\delta^{18}O$ measurements on *N. incompta* ($n = 5$) and *T. quinqueloba* ($n = 4$) specimens, the average standard deviations of replicate measurements were 0.23 and 0.22‰ respectively.

To generate a robust age model (Section 2.5), additional samples of the benthic foraminifera *C. wuellerstorfi* were hand-picked at the University of Salamanca (between 1 and 11 specimens per sample) and analyzed at the Leibniz Laboratory for Radiometric Dating and Isotope Research of the Christian-Albrechts University in Kiel. Stable isotope analyses were performed on a Thermo-Finnigan MAT 253 mass spectrometer coupled to a Kiel IV carbonate preparation device. The analytical precision of two international standards (NBS-19; IAEA-603) and three laboratory internal standards was better than ±0.08‰. Results are reported on the VPDB standard scale.

2.3. $\delta^{15}N$ Analysis of *N. incompta*

Sample preparation and measurement of foraminifera-bound $\delta^{15}N$ were carried out at the Ren lab, National Taiwan University, using the protocol described in Ren et al. (2017). The cleaning procedures include ultrasonicating the samples in 2% polyphosphate solution to dislodge and remove organic matter, attached to the surface of the shells. The foraminifera samples were then treated in bicarbonate-buffered dithionite—citric acid in an 80°C water bath for 1 hr. To eliminate nitrogen isotope contamination from the adsorbed particulate nitrogen on the shells, the samples were oxidized with high concentrations of basic potassium persulfate ("POR;" 50 g of potassium persulfate and 50 g of NaOH to 1 liter of Milli-Q) and autoclaved at 121°C for 1 hr. The cleaned samples were oven-dried for 48 hr, and subsequently weighed and transferred to pre-combusted 4 ml borosilicate glass vials with an aliquot size of ∼3 mg. The samples were then dissolved in 63 μL of 2N HCl. Subsequently, the trapped organic matter in the dissolved samples was oxidized to nitrate using 1 mL of recrystallized basic persulfate solution (0.3 g of potassium persulfate and 0.7 g of NaOH to 100 ml of Milli-Q) while autoclaved at 121°C for 1 hr on the slow-vent setting. To constrain the $\delta^{15}N$ blanks in persulfate solutions, two organic standards were prepared in three dilution ranges (2.5, 10, and 40 μL of nitrate concentration). We used organic standard USGS-40 ($\delta^{15}N = -4.52$‰ vs. air) and an internal mixture of six-aminocaproic acid and glycine ($\delta^{15}N = 5.4$‰ vs. air). Each batch of analysis contained eight POR blanks and a total of 12 organic standards. After the oxidation step, the samples were centrifuged and clear solutions were transferred to 4 ml pre-combusted borosilicate glass vials, followed by adjusting the pH of the basic sample solution between the range of 4–7 using 2N HCl.

At this step, nitrate concentrations were measured by reduction of nitrate to nitric oxide using a vanadium (III) solution heated to 100°C, followed by chemiluminescence detection (Braman & Hendrix, 1989). Based on

previous measurements on *N. incompta*, the nitrogen content in the foraminifera samples were assumed to be 3 nmol/mg (Studer et al., 2021). The nitrate concentration of the blank was found to be 0.1 μM, representing 1%–3% of the total nitrogen in the samples. The determination of $\delta^{15}N$ in the foraminifera samples, as well as the bacterial blanks and organic standards, was carried out using the denitrifier method in conjunction with gas chromatography (modified SigBench) and isotope ratio mass spectrometry (MAT 253 plus) (Weigand et al., 2016).

The denitrifying method uses a strain of *Pseudomonas chlororaphis* bacteria to convert dissolved nitrate and nitrite to nitrous oxide gas (Sigman et al., 2001). This denitrifying bacterium lacks the enzyme N_2O reductase. We added 1.5 ml of bacteria in pre-combusted 20 ml borosilicate vials and flushed the vials for 3 hr with N_2 gas. We then added sufficient volumes of our oxidized sample and standards, based on their nitrate concentration, to achieve 5 nmol of nitrogen and stored them overnight to ensure complete conversion of nitrate and nitrite to nitrous oxide. The success rate of the denitrifying method and the performance of the mass spectrometer was determined using nitrate reference materials IAEA-NO3 ($\delta^{15}N = 4.7‰$ vs. air), and USGS-34 ($\delta^{15}N = -1.8‰$ vs. air) at regular intervals. The oxidation standards were used to correct for the oxidation blanks.

Due to the small sample size and low nitrogen content within the foraminifera, duplicate samples were measured only for 11 samples with an average standard deviation of 0.28‰. The standard deviation (1σ) of the IAEA-N3 and USGS 34 standards was found to be 0.07 and 0.11‰, respectively. The standard deviation (1σ) of the organic standards analyzed alongside these samples was determined to be 0.2‰, which agrees with the long-term variability observed in-house using homogenized coral samples (±0.25‰). Therefore, we assume the analytical error for the $\delta^{15}N$ in our new record to be around 0.25–0.28‰ based on both replicate measurements and long-term in-house variability.

2.4. Calcareous Nannofossil Analysis

Ten samples were selected for analysis of the concentration of calcareous nannofossil particles (i.e., coccoliths) in sediments and the calculation of nannofossil accumulation rates. Sample selection followed the available age model in this study, with a resolution ranging between 3 and 10 kyr throughout the interval. The glass slides for microscopic analysis were prepared following the random settling technique by Flores and Sierro (1997). Nannofossil abundance was estimated by counting a minimum of 400 coccoliths in a variable number of fields of view, with the use of a double polarized–light microscope Nikon Eclipse 80i at 1000X. The total absolute nannofossil concentration per gram of sediment (N; nannofossil g^{-1} sediment) and nannofossil accumulation rates (NAR; coccolith cm^{-2} kyr^{-1}) profiles were calculated following the equations by Flores and Sierro (1997). NAR was calculated considering wet bulk density values for each sample from the shipboard Gamma Ray Attenuation and the sedimentation rates derived from the age model. N and NAR are commonly considered as an qualitative estimate of the changes in primary productivity at the surface most ocean layer, where coccolithophores inhabit (e.g., González-Lanchas, Flores, et al., 2021; González-Lanchas, Hernández-Almeida, et al., 2021; Stolz & Baumann, 2010).

2.5. Chronological Framework

The age model for the studied section (Figure 2) is based on a comparison of our benthic $\delta^{18}O$ record with the global benthic oxygen isotope stack from Lisiecki and Raymo (2005). QAnalySeries software (Kotov & Pälike, 2018) was used to identify the tie points used for the correlation between records (see online data). Between tie points, ages were calculated by linear interpolation (raw data can be found in the online data). All other cores presented in this study had their age model synchronized to the global benthic $\delta^{18}O$ stack chronology (Lisiecki & Raymo, 2005). We used the age model recently developed by Middleton et al. (2024) for ODP site 980.

3. Results and Discussion

3.1. Variations in Temperature, Salinity, and Seasonality Based on Planktic $\delta^{18}O$ and $\delta^{13}C$

In both foraminifera species, $\delta^{18}O$ values remained mostly stable at ~1.5–2.5‰, until a positive excursion from ~397 to 389 ka, during which values over 3‰ are reached (Figure 3c). Following 405 ka, intensified variability is observed concomitant with the large positive planktic $\delta^{18}O$ excursion. Variability in planktic $\delta^{18}O$ could reflect changes in upper-ocean temperature and/or salinity (Ravelo & Hillaire-Marcel, 2007). However, relatively stable

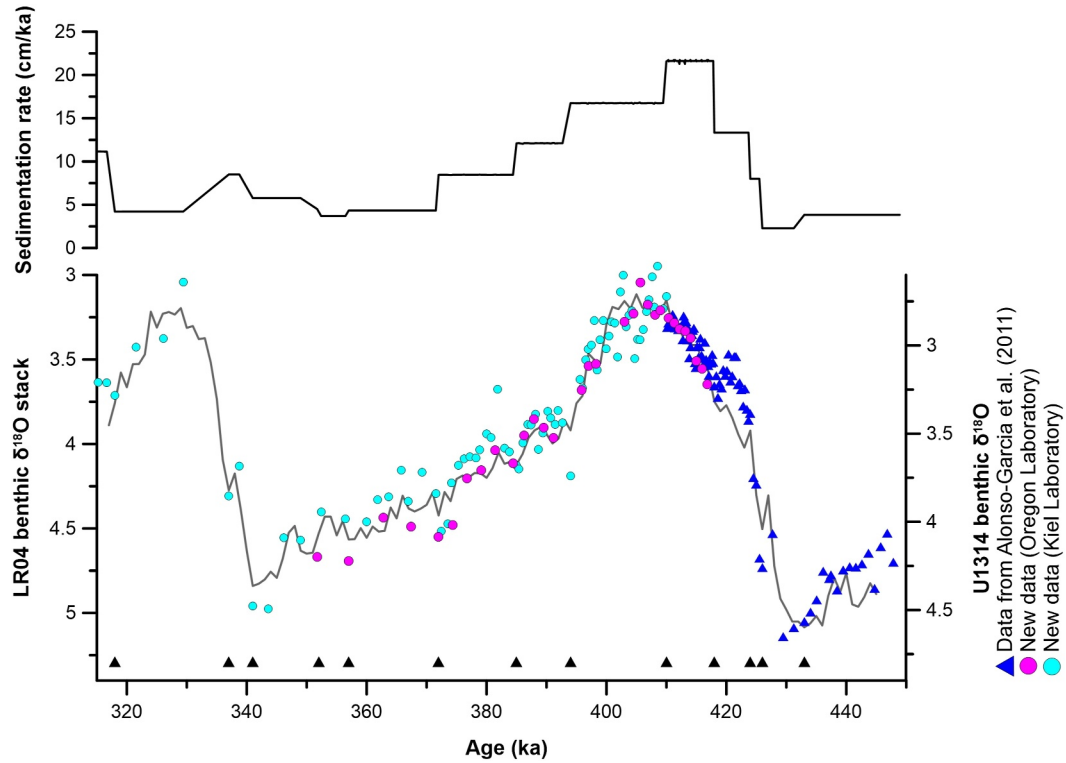

Figure 2. New age model and sedimentation rate at site U1314. Comparison of U1314 benthic $\delta^{18}O$ record with the benthic $\delta^{18}O$ stack (Lisiecki & Raymo, 2005) after performing the age model. Both records show similar $\delta^{18}O$ shifts. Black triangles indicate the positions of tie points.

$\delta^{18}O$ values in both *N. incompta* and *T. quinqueloba* U1314 record concomitant with sea-surface temperature (SST) variations on the order of ∼5°C (Alonso-Garcia, Sierro, Kucera, et al., 2011) argue against temperature being the main factor controlling these records over the 420–400 ka interval (Figure 3f). Over this period, the U1314 $\delta^{18}O$ record resembles the more-southern GIK23414-8 cores and U1305, which appears to track the classic shape of interglaciation (Figure 3c). However, the U1314 record displays persistently lower $\delta^{18}O$ values by about 0.4‰ than its southern counterpart, suggesting warmer and/or fresher conditions at site U1314 compared to GIK23414-8. Fresher conditions would be consistent with previous findings of a major northern input of freshwater during this period (Doherty & Thibodeau, 2018; Thibodeau et al., 2017). Following the climatic optimum, variability in planktic $\delta^{18}O$ values at U1314 appear to further differ from the rather gradual increase of planktic $\delta^{18}O$ values at GIK23414-8 (Figure 3c). Moreover, there is a large increase of about 2‰ in planktic $\delta^{18}O$ from ∼397 to 389 ka, which was not recorded at GIK23414-8 in the oxygen isotopic composition of either *G. bulloides* or the deeper-dwelling *N. pachyderma* (Figure 3c). These data suggest that intense cooling occurred at U1314 beginning at ∼397 ka, preceding the relatively subdued cooling at GIK23414-8. Interestingly, this cooling is associated with a resurgence of IRD (Figure 3g). While IRD is often associated with freshwater input, freshening is not recorded by $\delta^{18}O$. This could perhaps be because the freshwater signal is masked by a much stronger cooling of more than 6°C. Yet, planktic $\delta^{18}O$ at U1314 show a recovery to values similar to those observed at GIK23414-8 following this cooling interval, indicating that this was a regional and transient event rather than a return to a glacial climate (Figure 3c).

In the modern ocean, foraminifera species *N. incompta* and *T. quinqueloba* calcify at the bottom of the mixed layer (about 50 m), thus recording sea-surface conditions (Jonkers & Kučera, 2015; Jonkers et al., 2010; Kretschmer et al., 2018). While *N. incompta* flux peaks twice a year following primary productivity (during the spring bloom and summer; Chapman, 2010; Jonkers & Kučera, 2015), *T. quinqueloba* flux mostly peaks during summer time (Jonkers et al., 2010). However, *N. incompta* has only been recorded to bloom during summer at locations north of 55° in the modern ocean. Thus, its seasonality may change depending on climate as it prefers relatively warmer water (Chapman, 2010; Morley et al., 2017). Because different species of planktic foraminifera

10.1029/2024PA004935

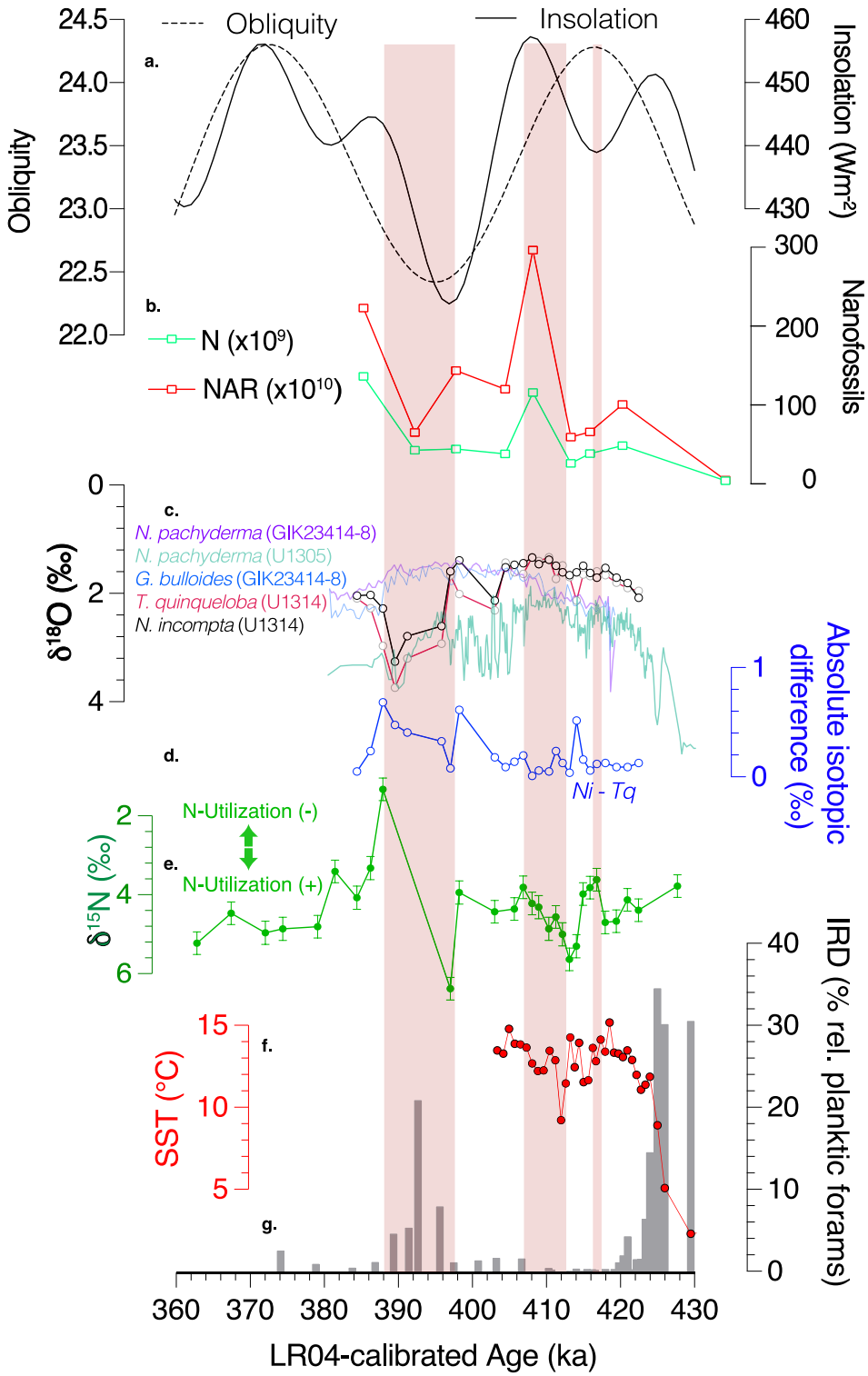

Figure 3. Results of coring site U1314. (a) Insolation at 65°N and obliquity (Berger & Loutre, 1991); (b) Relative changes in surface primary productivity at site U1314 from changes in nannofossil absolute concentration in sediments (N) and nannofossil accumulation rate (NAR; this study); (c) planktic $\delta^{18}O$ values from sites U1314 (this study), U1305 (Irvalı et al., 2020) and GIK23414-8 (Kandiano & Bauch, 2007); (d) Absolute difference in the $\delta^{18}O$ composition between Neogloboquadrina *incompta* and *Turborotalita quinqueloba* (this study); (d) $\delta^{15}N$ of *N. incompta* (this study); (f) Sea-surface temperature (SST) reconstructed via transfer functions (Alonso-Garcia, Sierro, Kucera, et al., 2011); and (g) Ice-rafted debris (IRD) % relative to planktic foraminifera from site U1314 (including data from Alonso-Garcia, Sierro, Kucera, et al., 2011). The red shaded areas highlight the three period of decrease in FB-$\delta^{15}N$ (discussed in Section 3.2–3.4).

can bloom at different times in the year, they can record surface and subsurface ocean conditions at these different bloom times (Metcalfe et al., 2019; Williams et al., 1981). Due to the difference in the timing of *N. incompta* blooms, which peak in spring and late summer, and *T. quinqueloba* blooms, which mostly occur in peak summer (Jonkers et al., 2010), the $\delta^{18}O$ offset between these species ($\Delta\delta^{18}O = \delta^{18}O_{T.\ quinqueloba} - \delta^{18}O_{N.\ incompta}$) can be used to estimate the seasonality at the bottom of the summer mixed layer. Offsets between $\delta^{18}O$ values are generally small until ~405 ka, except for ~415 ka, when values briefly increase to 0.5 and 0.3‰, respectively (Figure 3c). This increased offset is coincident with a simultaneous increase in the $\delta^{18}O$ of *T. quinqueloba*, which suggests that summer may have been particularly affected by cooling relative to spring. After 405 ka, isotopic offsets exhibit considerable variability and regularly reach values >0.3‰ for oxygen, again with *T. quinqueloba* being more enriched than *N. incompta*, suggesting increased seasonality.

3.2. Nutrient Utilization and Mixed-Layer Depth

The relative degree of nutrient consumption (nutrient utilization) controls the $\delta^{15}N$ of particulate organic matter (Altabet & Francois, 1994), as phytoplankton preferentially assimilate ^{14}N relative to ^{15}N when nutrient consumption is incomplete (e.g., under a deep mixed layer and high vertical nutrient supply). As nutrient consumption approaches completion, however, ^{15}N discrimination by phytoplankton becomes less expressed and the $\delta^{15}N$ of particulate organic matter increases. Heterotrophic planktic foraminifera such as *N. incompta* consume this organic matter and thus retain its nitrogen isotopic composition (Smart et al., 2018). Therefore, the foraminifera-bound $\delta^{15}N$ (FB-$\delta^{15}N$) signal integrates the relative proportion of nutrient assimilation (i.e., primary productivity) to nutrient supply. FB-$\delta^{15}N$ in the Iceland Basin and Nordic Seas have been previously interpreted to record changes in nutrient utilization driven by the depth of the summer mixed layer (Doherty et al., 2021; Straub et al., 2013). This is due to the fact that the depth of the mixed layer controls nutrient supply to the photic zone (Straub et al., 2013). Under a deep mixed layer, nutrient supply is high and the degree of nutrient consumption relative to nutrient supply is low (i.e., incomplete consumption). Assuming a constant level of productivity, a shallower MLD would result in a reduction in vertical nutrient supply and thus more complete nutrient consumption. Therefore, it is possible to use FB-$\delta^{15}N$ in conjunction with primary productivity proxies, here a micropaleontological coccolithophore-derived record, and other surface tracers to investigate variability in the upper ocean structure. While this proxy may be used to track N-supply and upper-ocean structure, it is important to exert caution as this signal may be altered by the increased dependence of phytoplankton on recycled ammonium which tends to lower the $\delta^{15}N$ of particulate organic matter toward the end of summer (Smart et al., 2018).

From ~428 to 405 ka, FB-$\delta^{15}N$ values varied between ~3 and 5.5‰, with a minimum around 414–416 ka and a maximum at 411 ka (Figure 3e). A large amplitude variation is observed from ~400 to 385 ka where values ranged from ~1.5 to more than 6‰, coincident also with the intensified variability of $\delta^{18}O$ isotopic offset between *N. incompta* and *T. quinqueloba* (Figure 3c) and the positive planktic $\delta^{18}O$ excursion (Figure 3a). A maximum FB-$\delta^{15}N$ value of 6.4‰ is observed at 397 ka, followed by a minimum value of 1.3‰ at 388 ka. This dramatic reduction in FB-$\delta^{15}N$, by ~5‰, is also coincident with the largest increase in $\delta^{18}O$ values (Figure 3a) of the record. However, the amplitude of this change is too large to be reasonably explained exclusively by changes in nutrient utilization. Rather, this extremely low value could be caused by an increased reliance of phytoplankton on ammonium at the end of the summer. This may be due to longer summer or also by the fact that *N. incompta* may have restricted its bloom period to summer, which may happen in colder conditions (Chapman, 2010; Morley et al., 2017). Moreover, because of the low abundance of foraminifera in this part of the core, this "peak" depends on a single point, which also calls for caution when interpreting this feature of the record. At ~385 ka, FB-$\delta^{15}N$ again stabilized and ranged from ~3 to 5‰ for the remainder of the record. In summary, at the U1314 location, temperature, stratification, and nutrient utilization exhibited a relatively consistent pattern, with lower amplitude variations from 425 to 400 ka and strong, larger variations from 400 to 385 ka.

3.3. Pre-Optimum Surface Conditions and Implications for Deep Water Ventilation

Prior to ~405 ka, planktic $\delta^{18}O$ values, absolute $\delta^{18}O$ differences, and FB-$\delta^{15}N$ remained relatively stable (Figures 3c–3e). However, we can highlight two episodes of decrease in FB-$\delta^{15}N$ from 418 to 416 ka and from 413 to 407 ka. Surface primary productivity levels remained relatively stable or increased during intervals for which there are coccolith data available (Figure 3b), indicating that the FB-$\delta^{15}N$ minima most likely reflect an increase in the MLD rather than decreased N consumption. Such increased MLD conditions may have relevance

for the strength of the AMOC, as decreased upper-ocean stratification could facilitate deep-water formation. Indeed, it was previously argued that a negative FB-δ^{15}N excursion in the Nordic Seas at core MD99-2277 (Figure 4c) corresponded to an increase in deep-water formation in the region, which strengthened the AMOC, from ~410 to 407 ka (Doherty et al., 2021). The two FB-δ^{15}N at site U1314 minima appears to occur simultaneously with an increase in the Atlantic benthic North Atlantic δ^{13}C stack, previously interpreted to reflect ventilation and AMOC strength (Lisiecki, 2010, 2014) (Figure 4i). It is therefore plausible that the Iceland Basin may have played an active role in deep-water formation, increasing the strength of the AMOC, prior to 405 ka. Furthermore, the onset of the peak benthic δ^{13}C in the North Atlantic stack (Figure 4) aligns with these findings, providing further support for the strong connectivity between surface conditions and deep-water ventilation. This reinforces the previous hypothesis regarding the significant role played by these regions in the initiation of the climate optimum of MIS 11 (Doherty et al., 2021). Interestingly, we observed no increase in the *C. wuellerstorfi* δ^{13}C at our IODP site U1314 during these two events. At IODP sites U1314 and U1313, the δ^{13}C reaches a plateau earlier (424 ka) than any other site we compiled (Figures 4d and 4e). IODP sites U1304 and U1305 reached their plateau right after (423 ka; Figure 4g) while δ^{13}C reached its first plateau around 419 ka at site ODP 980 (Figure 4f). The δ^{13}C is also enriched at IODP site U1314 (~0.8‰) and site U1305 (~0.7‰) compared to ODP site 980 (~0.4‰) (Figure 4), this may suggest that early formation of ISOW was mostly flowing in the route bathing sites U1314/05 and overflow downstream of the Wyville-Thomson Ridge only later in the interglacial. It could also be due to a later retreat of Antarctic Bottom Water following MIS 12 at ODP site 980. The absence of an increase in the benthic δ^{13}C signal at IODP site U1314 may be due to the already existing strong ventilation of deep water at that site (relatively high δ^{13}C) that could mask the signal of local deep-water formation.

3.4. Post-Optimum Cooling and Upper-Ocean Instability

After 405 ka, the δ^{18}O offset between *N. incompta* and *T. quinqueloba* varied between 0 and 0.6‰ with an average of 0.3‰, an higher average compared to the pre-optimum period (0.14‰) (Figure 3d). While our record does not possess the same resolution for FB-δ^{15}N during this period due to the lower occurrence of this foraminifera in the samples, we observe larger amplitude variation of FB-δ^{15}N values compared to the pre-optimum period (Figure 3e). These large variations suggest changes in stratification and mixed layer depth but may also involve a change in the blooming period of *N. incompta*. While productivity increases as well (Figure 3b), it would have the opposite effect on nutrient utilization and on FB-δ^{15}N and therefore should not be the main driver of the signal. The synchronicity between the less complete nutrient utilization (low FB-δ^{15}N) and the enhanced seasonality (high $\Delta\delta^{18}$O), argues for a control of the changes in the upper-ocean structure on these data. The main feature is a strong change in most surface proxies from 396 to 386 ka, where the δ^{18}O of both *N. incompta* and *T. quinqueloba* displays a very similar trend of stepwise-like enrichment. This suggests a transition toward colder and/or saltier waters starting around the time of the lowest insolation and obliquity of MIS 11 (396 ka; Figure 3a). At the start of this event we observe depleted planktic δ^{18}O, high FB-δ^{15}N, and highly ventilated deep water at our site as indicated by high benthic δ^{13}C (Figure 4d). This also corresponds to the first post-climate optimum occurrence of IRD at site U1314 (Figure 3f) and site ODP 980 (Oppo et al., 1998), and a doubling of the IRD found at site MD99-2277 (not shown, Doherty et al., 2021). Progressing into the event there is an enrichment in δ^{18}O peaking around 388 ka (Figure 3c), synchronously to this enrichment and its peak we observe a depletion in FB-δ^{15}N (Figure 3e), an increase in $\Delta\delta^{18}$O (Figure 3d) and a decrease in benthic δ^{13}C in the North Atlantic benthic δ^{13}C stack (Figure 4i). This cooling event even affected the North Atlantic mid-latitudes reaching the Iberian margin where SST dropped (Rodrigues et al., 2017) and the vegetation of the Iberian Peninsula shows a shift toward colder and drier taxa (Oliveira et al., 2016). Moreover, ODP Site 980 is also characterized by bottom water change, as both benthic δ^{13}C (Figures 4f, Oppo et al., 1998) and Nd isotopes (not shown; Link, 2022) show trend indicating the presence of cooler/saltier, less ventilated and more radiogenic bottom waters, which may suggest a temporary weakening of deep water formation. These features are also coherent with a dip in the North Atlantic benthic δ^{13}C stack (Lisiecki, 2010; Figure 4i).

The post-climate optimum minimum recorded in the FB-δ^{15}N is thus very different from the minima occurring in the earlier part of the interglacial as our proxy data indicates cold conditions and presence of IRD from 398 to 389 ka that seem to have impeded deep-water formation. This suggests that while upper-ocean stratification may have changed before or during the climate optimum, a threshold in temperature and/or stratification was not reached to have significantly reduced the formation of deep water.

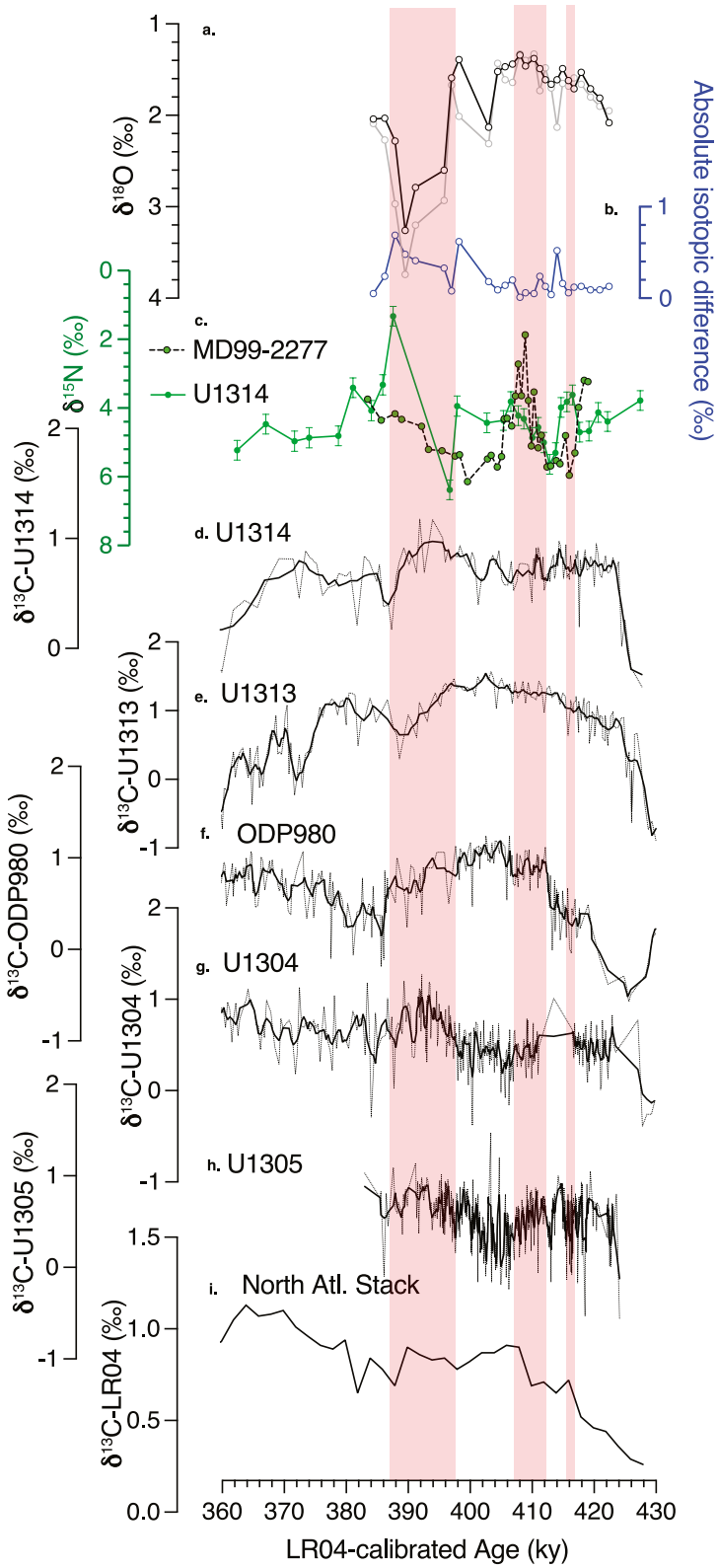

Figure 4.

3.5. Connectivity With the Subpolar Gyre and Labrador Sea Deep Water Ventilation

To better understand the potential causes and consequences of these post-climate optimum upper-ocean instabilities we expand our comparisons to sites within the subpolar gyre. The enriched $\delta^{18}O$ excursion of about 2.5‰ observed in IODP site U1314 from 398 to 390 ka is less pronounced, but present, in IODP site U1305 further along the northern path of the subpolar gyre but not in core GIK23414-8 (Figure 3c), which is southward of site U1314 and influenced by the NAC (Figure 1). Since this excursion is synchronous with the regional reappearance of IRD, as mentioned in the previous section, it is possible that this feature is associated with cooling and presence of icebergs in the Iceland basin and the subpolar gyre. Interestingly, the decrease in deep water ventilation that was observed in North Atlantic was not observed in the Labrador Sea during this period at IODP site U1305 (Figure 4h). During this episode, IODP site U1305 is characterized by the highest $\delta^{13}C$ of the MIS 11 record, higher than peak interglacial values, indicating highly ventilation bottom waters. This may suggest that the proportion of deep-water formed in different basins changed throughout the interglacial, with stronger relative contribution from the Nordic Seas, or eastern part of the North Atlantic Deep Water from about 410 ka until the end of the cold event spanning 398–386 ka.

Our data thus provide compelling evidence of a complex connection linking surface instability in the Iceland basin to deep water ventilation within the North Atlantic and Labrador Sea via the subpolar gyre circulation. Our findings also support previous hypotheses suggesting that the subpolar gyre may be more sensitive to changes in the Arctic front compared to the North Atlantic Current (Alonso-Garcia, Sierro, & Flores, 2011; Barker et al., 2015).

4. Concluding Remarks

Our multiproxy study of MIS 11 in the Iceland Basin reveals significant upper-ocean instability and its connection to changes in deep-water ventilation during this unusually extended interglacial period. The key findings and interpretations from our study are:

1. We identified a relatively stable pre-climate optimum period (425–405 ka) and an unstable post-climate optimum period (405–385 ka) characterized by high-amplitude variations in nutrient utilization and seasonality proxies.
2. Prior to 405 ka, we observed two episodes of decreased foraminifera-bound $\delta^{15}N$ (FB-$\delta^{15}N$), which we interpret to indicate deeper summertime mixed layers that preconditioned the water column for wintertime deep water formation. These episodes coincided with increases in the North Atlantic benthic $\delta^{13}C$ stack, suggesting that the Iceland Basin may have played an active role in deep-water formation and AMOC strengthening during this period.
3. After 405 ka, we observed larger variations in FB-$\delta^{15}N$ and increased seasonality, indicating changes in upper-ocean structure. A notable cooling event from 396 to 386 ka was characterized by enriched $\delta^{18}O$, depleted FB-$\delta^{15}N$, increased IRD, and decreased benthic $\delta^{13}C$ across multiple North Atlantic sites.
4. While the cooling event was associated with decreased deep-water ventilation in much of the North Atlantic, the Labrador Sea (site U1305) showed highly ventilated bottom waters during this period, highlighting the complex spatial dynamics of deep-water formation.
5. Our data support the hypothesis that the subpolar gyre may be more sensitive to changes in the Arctic front compared to the North Atlantic Current, as evidenced by the varying responses across different core sites.

These findings have important implications for our understanding of ocean circulation and climate dynamics. Our study suggests that deep-water formation was not uniformly strong throughout MIS 11, but rather varied in intensity and location depending on regional surface conditions. The complex relationships observed between surface conditions, deep-water ventilation, and regional differences highlight the need for a comprehensive

Figure 4. Comparison of sea-surface proxy, and deep-water ventilation. From the top of the figure: (a) Planktic $\delta^{18}O$ values in *Neogloboquadrina incompta* (black) and *Turborotalita quinqueloba* (gray) (this study); (b) absolute difference in the $\delta^{18}O$ composition between *N. incompta* and *T. quinqueloba* (this study); (c) $\delta^{15}N$ of *N. incompta* from site U1314 (this study) and of *N. pachyderma* from site MD99-2277 (Nordic Seas); (Doherty et al., 2021); (d) benthic $\delta^{13}C$ record from coring IODP site U1314 (2820 m depth, this study); (e) site U1313 (3,420 m depth, Voelker et al., 2010); (f) ODP site 980 (2,270 m depth, Middleton et al., 2024; Oppo et al., 1998); (g) site U1304 (3,024 m depth, Hodell & Channell, 2016; Xuan et al., 2016); (h) site U1305 (3,549 m depth, Galaasen et al., 2020); (i) and the North Atlantic benthic stack indicative of AMOC strength (1,145–4,620 m depth, Lisiecki, 2010, 2014). Red bands indicate the main periods of decreasing FB-$\delta^{15}N$ recorded at IODP site U1314.

approach in reconstructing past ocean circulation patterns. As MIS 11 is considered a potential analog for future warm climate states, our findings suggest that the response of deep-water formation to warming may be spatially and temporally variable, rather than following a simple strengthening or weakening pattern. Furthermore, the study underscores the importance of using multiple proxies and considering regional contexts when interpreting paleoceanographic data, particularly for complex periods like MIS 11.

Data Availability Statement

Original data can be found in the CUHK data repository (Thibodeau, 2025).

Acknowledgments

This study was funded through the General Research Fund from the Research Grant Council of Hong Kong (17301818, 17301320) awarded to BT. We are thankful to undergraduate Yuet F. Ling for help picking foraminifera for the $\delta^{15}N$ and to Jennifer McKay (Oregon State University) for the $\delta^{18}O$ and $\delta^{13}C$ analysis. We also acknowledge Nils Anderson's help with the stable isotopes analysis (University of Kiel). MAG acknowledges funding from the Spanish Government through the project PICTURE (PID2021-128322NB-I00). Thanks to IODP for providing the samples for this study. We thank David Thornalley for his comment on the thesis version of the paper. We also thank Jesse Farmer and two anonymous reviewers for their constructive comments.

References

Alonso-Garcia, M., Sierro, F. J., & Flores, J. A. (2011). Arctic front shifts in the subpolar North Atlantic during the Mid-Pleistocene (800–400 ka) and their implications for ocean circulation. *Palaeogeography, Palaeoclimatology, Palaeoecology*, *311*(3), 268–280. https://doi.org/10.1016/j.palaeo.2011.09.004

Alonso-Garcia, M., Sierro, F. J., Kucera, M., Flores, J. A., Cacho, I., & Andersen, N. (2011). Ocean circulation, ice sheet growth and interhemispheric coupling of millennial climate variability during the mid-Pleistocene (ca 800–400 ka). *Quaternary Science Reviews*, *30*(23), 3234–3247. https://doi.org/10.1016/j.quascirev.2011.08.005

Altabet, M. A., & Francois, R. (1994). Sedimentary nitrogen isotopic ratio as a recorder for surface ocean nitrate utilization. *Global Biogeochemical Cycles*, *8*(1), 103–116. https://doi.org/10.1029/93GB03396

Barker, S., Chen, J., Gong, X., Jonkers, L., Knorr, G., & Thornalley, D. (2015). Icebergs not the trigger for North Atlantic cold events. *Nature*, *520*(7547), 333–336. https://doi.org/10.1038/nature14330

Bauch, H. A., Kandiano, E. S., Helmke, J., Andersen, N., Rosell-Mele, A., & Erlenkeuser, H. (2011). Climatic bisection of the last interglacial warm period in the Polar North Atlantic. *Quaternary Science Reviews*, *30*(15–16), 1813–1818. https://doi.org/10.1016/j.quascirev.2011.05.012

Berger, A., & Loutre, M. F. (1991). Insolation values for the climate of the last 10 million years. *Quaternary Science Reviews*, *10*(4), 297–317. https://doi.org/10.1016/0277-3791(91)90033-Q

Berger, A., & Loutre, M. F. (2002). An exceptionally long interglacial ahead? *Science*, *297*(5585), 1287–1288. https://doi.org/10.1126/science.1076120

Bianchi, G. G., & McCave, I. N. (2000). Hydrography and sedimentation under the deep western boundary current on Bjorn and Gardar Drifts, Iceland Basin. *Marine Geology*, *165*(1–4), 137–169. https://doi.org/10.1016/S0025-3227(99)00139-5

Braman, R. S., & Hendrix, S. A. (1989). Nanogram nitrite and nitrate determination in environmental and biological materials by vanadium(III) reduction with chemiluminescence detection. *Analytical Chemistry*, *61*(24), 2715–2718. https://doi.org/10.1021/ac00199a007

Buckley, M. W., & Marshall, J. (2016). Observations, inferences, and mechanisms of the Atlantic meridional overturning circulation: A review. *Reviews of Geophysics*, *54*(1), 5–63. https://doi.org/10.1002/2015RG000493

Candy, I., Schreve, D. C., Sherriff, J., & Tye, G. J. (2014). Marine Isotope Stage 11: Palaeoclimates, palaeoenvironments and its role as an analogue for the current interglacial. *Earth-Science Reviews*, *128*, 18–51. https://doi.org/10.1016/j.earscirev.2013.09.006

Chapman, M. R. (2010). Seasonal production patterns of planktonic foraminifera in the NE Atlantic Ocean: Implications for paleotemperature and hydrographic reconstructions. *Paleoceanography*, *25*(1). https://doi.org/10.1029/2008PA001708

Coplen, T. (1995). Discontinuance of SMOW and PDB. *Nature*, *375*, 285. https://doi.org/10.1038/375285a0

Denton, G. H., Anderson, R. F., Toggweiler, J. R., Edwards, R. L., Schaefer, J. M., & Putnam, A. E. (2010). The last glacial termination. *Science*, *328*(5986), 1652–1656. https://doi.org/10.1126/science.1184119

de Vernal, A., & Hillaire-Marcel, C. (2008). Natural variability of greenland climate, vegetation, and ice volume during the past million years. *Science*, *320*(5883), 1622–1625. https://doi.org/10.1126/science.1153929

Dickson, A. J., Beer, C. J., Dempsey, C., Maslin, M. A., Bendle, J. A., McClymont, E. L., & Pancost, R. D. (2009). Oceanic forcing of the marine isotope stage 11 interglacial. *Nature Geoscience*, *2*(6), 428–433. https://doi.org/10.1038/ngeo527

Doherty, J. M., Ling, Y. F., Not, C., Erler, D., Bauch, H. A., Paytan, A., & Thibodeau, B. (2021). Freshening, stratification and deep-water formation in the Nordic Seas during marine isotope stage 11. *Quaternary Science Reviews*, *272*, 107231. https://doi.org/10.1016/j.quascirev.2021.107231

Doherty, J. M., & Thibodeau, B. (2018). Cold water in a warm world: Investigating the origin of the Nordic Seas' unique surface properties during MIS 11. *Frontiers in Marine Science*, *5*, 251. https://doi.org/10.3389/fmars.2018.00251

Droxler, A. W., Alley, R. B., Howard, W. R., Poore, R. Z., Burckle, L. H., & others (2003). Unique and exceptionally long interglacial marine isotope stage 11: Window into Earth warm future climate. *Geophysical Monograph*, *137*, 1–14. https://doi.org/10.1029/137GM01

Flores, J. A., & Sierro, F. J. (1997). Revised technique for calculation of calcareous nannofossil accumulation rates. *Micropaleontology*, *43*(3), 321–324. https://doi.org/10.2307/1485832

Galaasen, E. V., Ninnemann, U. S., Kessler, A., Irvalı, N., Rosenthal, Y., Tjiputra, J., et al. (2020). Interglacial instability of North Atlantic Deep Water ventilation. *Science*, *367*(6485), 1485–1489. https://doi.org/10.1126/science.aay6381

González-Lanchas, A., Flores, J.-A., Sierro, F. J., Sánchez Goñi, M. F., Rodrigues, T., Ausín, B., et al. (2021). Control mechanisms of primary productivity revealed by calcareous nannoplankton from marine isotope stages 12 to 9 at the Shackleton Site (IODP Site U1385). *Paleoceanography and Paleoclimatology*, *36*(6), e2021PA004246. https://doi.org/10.1029/2021PA004246

González-Lanchas, A., Hernández-Almeida, I., Flores, J.-A., Sierro, F. J., Guitian, J., & Stoll, H. M. (2021). Carbon Isotopic Fractionation of Alkenones and *Gephyrocapsa* Coccoliths Over the Late Quaternary (Marine Isotope Stages 12–9) Glacial-Interglacial Cycles at the Western Tropical Atlantic. *Paleoceanography and Paleoclimatology*, *36*(8), e2020PA004175. https://doi.org/10.1029/2020PA004175

Hodell, D. A., & Channell, J. E. T. (2016). Mode transitions in Northern Hemisphere glaciation: Co-evolution of millennial and orbital variability in Quaternary climate. *Climate of the Past*, *12*(9), 1805–1828. https://doi.org/10.5194/cp-12-1805-2016

Imbrie, J., Berger, A., Boyle, E. A., Clemens, S. C., Duffy, A., Howard, W. R., et al. (1993). On the structure and origin of major glaciation cycles 2. The 100,000-year cycle. *Paleoceanography*, *8*(6), 699–735. https://doi.org/10.1029/93pa02751

Imbrie, J., Boyle, E. A., Clemens, S. C., Duffy, A., Howard, W. R., Kukla, G., et al. (1992). On the structure and origin of major glaciation cycles 1. Linear responses to Milankovitch forcing. *Paleoceanography*, *7*(6), 701–738. https://doi.org/10.1029/92PA02253

Irvalı, N., Galaasen, E. V., Ninnemann, U. S., Rosenthal, Y., Born, A., & Kleiven, H. K. F. (2020). A low climate threshold for south Greenland Ice Sheet demise during the Late Pleistocene. *Proceedings of the National Academy of Sciences of the United States of America*, *117*(1), 190–195. https://doi.org/10.1073/pnas.1911902116

Jonkers, L., Brummer, G.-J. A., Peeters, F. J. C., Van Aken, H. M., & De Jong, M. F. (2010). Seasonal stratification, shell flux, and oxygen isotope dynamics of left-coiling *N. pachyderma* and *T. quinqueloba* in the western subpolar North Atlantic: Seasonal foraminiferal fluxes and $\delta^{18}O$. *Paleoceanography*, *25*(2). https://doi.org/10.1029/2009PA001849

Jonkers, L., & Kučera, M. (2015). Global analysis of seasonality in the shell flux of extant planktonic Foraminifera. *Biogeosciences*, *12*(7), 2207–2226. https://doi.org/10.5194/bg-12-2207-2015

Kandiano, E. S., & Bauch, H. A. (2007). Phase relationship and surface water mass change in the Northeast Atlantic during marine isotope stage 11 (MIS 11). *Quaternary Research*, *68*(3), 445–455. https://doi.org/10.1016/j.yqres.2007.07.009

Kandiano, E. S., van der Meer, M. T. J., Schouten, S., Fahl, K., Sinninghe Damsté, J. S., & Bauch, H. A. (2017). Response of the North Atlantic surface and intermediate ocean structure to climate warming of MIS 11. *Scientific Reports*, *7*(1), 46192. https://doi.org/10.1038/srep46192

Killworth, P. D. (1983). Deep convection in the world ocean. *Reviews of Geophysics*, *21*(1), 1–26. https://doi.org/10.1029/RG021i001p00001

Kotov, S., & Pälike, H. (2018). QAnalySeries-a cross-platform time series tuning and analysis tool. In *AGU Fall Meeting Abstracts, 2018* (p. PP53D-1230). Retrieved from https://ui.adsabs.harvard.edu/abs/2018AGUFMPP53D1230K/abstract

Kretschmer, K., Jonkers, L., Kucera, M., & Schulz, M. (2018). Modeling seasonal and vertical habitats of planktonic foraminifera on a global scale. *Biogeosciences*, *15*(14), 4405–4429. https://doi.org/10.5194/bg-15-4405-2018

Link, J. M. (2022). Atlantic deep circulation during marine isotope stage 11 and the last one million years Inferred from neodymium isotopes [Dissertation]. https://doi.org/10.11588/heidok.00032226

Lique, C., Johnson, H. L., & Plancherel, Y. (2018). Emergence of deep convection in the Arctic Ocean under a warming climate. *Climate Dynamics*, *50*(9–10), 3833–3847. https://doi.org/10.1007/s00382-017-3849-9

Lique, C., & Thomas, M. D. (2018). Latitudinal shift of the Atlantic Meridional Overturning Circulation source regions under a warming climate. *Nature Climate Change*, *8*(11), 1013–1020. https://doi.org/10.1038/s41558-018-0316-5

Lisiecki, L. E. (2010). A benthic $\delta^{13}C$-based proxy for atmospheric pCO_2 over the last 1.5 Myr. *Geophysical Research Letters*, *37*(21), 1–5. https://doi.org/10.1029/2010GL045109

Lisiecki, L. E. (2014). Atlantic overturning responses to obliquity and precession over the last 3 Myr. *Paleoceanography*, *29*(2), 71–86. https://doi.org/10.1002/2013PA002505

Lisiecki, L. E., & Raymo, M. E. (2005). A Pliocene-Pleistocene stack of 57 globally distributed benthic $\delta^{18}O$ records. *Paleoceanography*, *20*(1), 1–17. https://doi.org/10.1029/2004PA001071

Loutre, M. F., & Berger, A. (2003). Marine Isotope Stage 11 as an analogue for the present interglacial. *Global and Planetary Change*, *36*(3), 209–217. https://doi.org/10.1016/S0921-8181(02)00186-8

Metcalfe, B., Feldmeijer, W., & Ganssen, G. M. (2019). Oxygen isotope variability of planktonic foraminifera provide clues to past upper ocean seasonal variability. *Paleoceanography and Paleoclimatology*, *34*(3), 374–393. https://doi.org/10.1029/2018PA003475

Middleton, J. L., Gottschalk, J., Winckler, G., Hanley, J., Knudson, C., Farmer, J. R., et al. (2024). Evaluating manual versus automated benthic foraminiferal $\delta^{18}O$ alignment techniques for developing chronostratigraphies in marine sediment records. *Geochronology*, *6*(2), 125–145. https://doi.org/10.5194/gchron-6-125-2024

Morley, A., Babila, T. L., Wright, J., Ninnemann, U., Kleiven, K., Irvali, N., & Rosenthal, Y. (2017). Environmental controls on Mg/Ca in *Neogloboquadrina incompta*: A core-top study from the subpolar North Atlantic. *Geochemistry, Geophysics, Geosystems*, *18*(12), 4276–4298. https://doi.org/10.1002/2017GC007111

Oliveira, D., Desprat, S., Rodrigues, T., Naughton, F., Hodell, D., Trigo, R., et al. (2016). The complexity of millennial-scale variability in southwestern Europe during MIS 11. *Quaternary Research*, *86*(3), 373–387. https://doi.org/10.1016/j.yqres.2016.09.002

Oppo, D. W., McManus, J. F., & Cullen, J. L. (1998). Abrupt climate events 500,000 to 340,000 Years Ago: Evidence from subpolar North Atlantic sediments. *Science*, *279*(5355), 1335–1338. https://doi.org/10.1126/science.279.5355.1335

Peacock, S., Lane, E., & Restrepo, J. M. (2006). A possible sequence of events for the generalized glacial-interglacial cycle. *Global Biogeochemical Cycles*, *20*(2). https://doi.org/10.1029/2005GB002448

Petit, T., Lozier, M. S., Josey, S. A., & Cunningham, S. A. (2020). Atlantic deep water formation occurs primarily in the Iceland Basin and irminger sea by local buoyancy forcing. *Geophysical Research Letters*, *47*(22). https://doi.org/10.1029/2020GL091028

Proceedings of the IODP, 303/306. (2006). *Proceedings of the IODP, 303/306*. Integrated Ocean Drilling Program. https://doi.org/10.2204/iodp.proc.303306.2006

Ravelo, A. C., & Hillaire-Marcel, C. (2007). The Use of oxygen and carbon isotopes of foraminifera in Paleoceanography. In *Developments in marine geology* (pp. 735–764). https://doi.org/10.1016/S1572-5480(07)01023-8

Raymo, M. E. (1997). The timing of major climate terminations. *Paleoceanography*, *12*(4), 577–585. https://doi.org/10.1029/97PA01169

Raynaud, D., Barnola, J.-M., Souchez, R., Lorrain, R., Petit, J.-R., Duval, P., & Lipenkov, V. Y. (2005). Palaeoclimatology: The record for marine isotopic stage 11. *Nature*, *436*(7047), 39–40. https://doi.org/10.1038/43639b

Ren, H., Sigman, D. M., Martínez-García, A., Anderson, R. F., Chen, M.-T., Ravelo, A. C., et al. (2017). Impact of glacial/interglacial sea level change on the ocean nitrogen cycle. *Proceedings of the National Academy of Sciences of the United States of America*, *114*(33), 201701315. https://doi.org/10.1073/pnas.1701315114

Reyes, A. V., Carlson, A. E., Beard, B. L., Hatfield, R. G., Stoner, J. S., Winsor, K., et al. (2014). South Greenland ice-sheet collapse during marine isotope stage 11. *Nature*, *510*(7506), 525–528. https://doi.org/10.1038/nature13456

Rodrigues, T., Alonso-García, M., Hodell, D. A., Rufino, M., Naughton, F., Grimalt, J. O., et al. (2017). A 1-Ma record of sea surface temperature and extreme cooling events in the North Atlantic: A perspective from the Iberian Margin. *Quaternary Science Reviews*, *172*, 118–130. https://doi.org/10.1016/j.quascirev.2017.07.004

Ruddiman, W. F. (1977). Late Quaternary deposition of ice-rafted sand in the subpolar North Atlantic (lat 40° to 65°N). *Bulletin of the Geological Society of America*, *88*(12), 1813–1827. https://doi.org/10.1130/0016-7606(1977)88<1813:LQDOIS>2.0.CO;2

Siegenthaler, U., Stocker, T. F., Monnin, E., Lüthi, D., Schwander, J., Stauffer, B., et al. (2005). Stable carbon cycle—Climate relationship during the late Pleistocene. *Science*, *310*(5752), 1313–1317. https://doi.org/10.1126/science.1120130

Sigman, D. M., Casciotti, K. L., Andreani, M., Barford, C., Galanter, M., Bhlke, J. K., et al. (2001). A bacterial method for the nitrogen isotopic analysis of nitrate in seawater and freshwater. *Analytical Chemistry*, *73*(17), 4145–4153. https://doi.org/10.1021/ac010088e

Simstich, J., Lorenz, S. J., & Bauch, H. A. (2012). Evaluation of past stratification changes in the Nordic Seas by comparing planktonic foraminiferal $\delta^{18}O$ with a solar-forced model. *Marine Micropaleontology*, *94–95*, 91–96. https://doi.org/10.1016/j.marmicro.2012.06.006

Simstich, J., Sarnthein, M., & Erlenkeuser, H. (2003). Paired $\delta^{18}O$ signals of *Neogloboquadrina pachyderma* (s) and *Turborotalita quinqueloba* show thermal stratification structure in Nordic Seas. *Marine Micropaleontology*, *48*(1–2), 107–125. https://doi.org/10.1016/S0377-8398(02)00165-2

Smart, S. M., Ren, H., Fawcett, S. E., Schiebel, R., Conte, M., Rafter, P. A., et al. (2018). Ground-truthing the planktic foraminifer-bound nitrogen isotope paleo-proxy in the Sargasso Sea. *Geochimica et Cosmochimica Acta*, *235*, 463–482. https://doi.org/10.1016/j.gca.2018.05.023

Stolz, K., & Baumann, K.-H. (2010). Changes in palaeoceanography and palaeoecology during Marine Isotope Stage (MIS) 5 in the eastern North Atlantic (ODP Site 980) deduced from calcareous nannoplankton observations. *Palaeogeography, Palaeoclimatology, Palaeoecology*, *292*(1), 295–305. https://doi.org/10.1016/j.palaeo.2010.04.002

Straub, M., Tremblay, M. M., Sigman, D. M., Studer, A. S., Ren, H., Toggweiler, J. R., & Haug, G. H. (2013). Nutrient conditions in the subpolar North Atlantic during the last glacial period reconstructed from foraminifera-bound nitrogen isotopes. *Paleoceanography*, *28*(1), 79–90. https://doi.org/10.1002/palo.20013

Studer, A. S., Mekik, F., Ren, H., Hain, M. P., Oleynik, S., Martínez-García, A., et al. (2021). Ice age-holocene similarity of foraminifera-bound nitrogen isotope ratios in the eastern equatorial Pacific. *Paleoceanography and Paleoclimatology*, *36*(5), e2020PA004063. https://doi.org/10.1029/2020PA004063

Thibodeau, B. (2025). Upper ocean instability in the subpolar North Atlantic and its implications for deep water formation during interglacials [Dataset]. *CUHK Research Data Repository. V1*. https://doi.org/10.48668/9AKTCT

Thibodeau, B., Bauch, H. A., & Pedersen, T. F. (2017). Stratification-induced variations in nutrient utilization in the Polar North Atlantic during past interglacials. *Earth and Planetary Science Letters*, *457*, 127–135. https://doi.org/10.1016/j.epsl.2016.09.060

Tzedakis, P. C., Hodell, D. A., Nehrbass-Ahles, C., Mitsui, T., & Wolff, E. W. (2022). Marine isotope stage 11c: An unusual interglacial. *Quaternary Science Reviews*, *284*, 107493. https://doi.org/10.1016/j.quascirev.2022.107493

Van Aken, H. M., & De Boer, C. J. (1995). On the synoptic hydrography of intermediate and deep water masses in the Iceland Basin. *Deep-Sea Research Part I*, *42*(2), 165–189. https://doi.org/10.1016/0967-0637(94)00042-Q

Vázquez Riveiros, N., Waelbroeck, C., Skinner, L., Duplessy, J.-C., McManus, J. F., Kandiano, E. S., & Bauch, H. A. (2013). The "MIS 11 paradox" and ocean circulation: Role of millennial scale events. *Earth and Planetary Science Letters*, *371*(372), 258–268. https://doi.org/10.1016/j.epsl.2013.03.036

Voelker, A. H. L., Rodrigues, T., Billups, K., Oppo, D., McManus, J., Stein, R., et al. (2010). Variations in mid-latitude North Atlantic surface water properties during the mid-Brunhes (MIS 9–14) and their implications for the thermohaline circulation. *Climate of the Past*, *6*(4), 531–552. https://doi.org/10.5194/cp-6-531-2010

Weigand, M. A., Foriel, J., Barnett, B., Oleynik, S., & Sigman, D. M. (2016). Updates to instrumentation and protocols for isotopic analysis of nitrate by the denitrifier method. *Rapid Communications in Mass Spectrometry*, *30*(12), 1365–1383. https://doi.org/10.1002/rcm.7570

Williams, D. F., Bé, A. W. H., & Fairbanks, R. G. (1981). Seasonal stable isotopic variations in living planktonic foraminifera from Bermuda plankton tows. *Palaeogeography, Palaeoclimatology, Palaeoecology*, *33*(1), 71–102. https://doi.org/10.1016/0031-0182(81)90033-X

Xuan, C., Channell, J. E. T., & Hodell, D. A. (2016). Quaternary magnetic and oxygen isotope stratigraphy in diatom-rich sediments of the southern Gardar Drift (IODP Site U1304, North Atlantic). *Quaternary Science Reviews*, *142*, 74–89. https://doi.org/10.1016/j.quascirev.2016.04.010

Zhuravleva, A., Bauch, H. A., & Van Nieuwenhove, N. (2017). Last Interglacial (MIS5e) hydrographic shifts linked to meltwater discharges from the East Greenland margin. *Quaternary Science Reviews*, *164*, 95–109. https://doi.org/10.1016/j.quascirev.2017.03.026